ADVANCED OPTICAL MATERIALS
www.advopticalmat.de

Angle-Tolerant Circular Eigenpolarizations Enabled by Orientational Disorder in Dielectric Metasurfaces

Katsuya Tanaka, Aso Rahimzadegan, Dennis Arslan, Anna Fitriana, Stefan Fasold, Dmitry Pidgayko, Michael Steinert, Thomas Pertsch, Manuel Decker, Carsten Rockstuhl, and Isabelle Staude*

Tailored structural disorder in photonic metasurfaces enables advanced light shaping. Specifically, an orientational disorder in chiral nanostructures leads to circular eigenpolarizations with a heavily suppressed linear birefringence. The orientational disorder is, therefore, vital to observing purely chiroptical effects such as circular dichroism and optical activity. Here, it is experimentally and numerically demonstrated that all-dielectric orientationally disordered chiral bilayer square array metasurfaces preserve highly circular eigenpolarizations for a wide range of incidence angles. The angle-dependent performance of disordered chiral metasurfaces is compared with that of their C_2 and C_4 symmetric periodic counterparts, demonstrating that the disordered structures provide nearly pure circular eigenpolarizations across a larger range of angles and wavelengths, whereas the periodic ones do not. These findings underscore the ability of tailored disorder to enhance the robustness of engineered chiroptical responses of all-dielectric metasurfaces and highlight its potential for flat, integrable, and highly efficient optical components, such as circular polarizers and beam splitters.

1. Introduction

Photonic metasurfaces are powerful tools for manipulating light at subwavelength scales, offering precise control over wavefronts, spectra, and polarization.[1–5] Traditionally, these metasurfaces are designed with periodic and ordered arrangements, as a disorder often leads to increased incoherent scattering, degrading the optical performance.[6,7] Moreover, theoretical and numerical modeling of disordered structures is challenging, which has limited the investigation of disordered metasurfaces.[6,7] However, reliance on periodicity limits the potential to explore a range of complex optical phenomena observed in disordered systems. Recent studies suggest that controlled disorder in photonic metasurfaces can enhance functionalities, such as increasing channel capacity, suppressing unwanted anisotropy, and enabling high numerical aperture (NA) focusing and fluorescent imaging.[7–10] Additionally, disorder-induced phase transitions in dielectric Huygens' metasurfaces and resonant near-perfect optical diffusers have demonstrated the potential of structural disorder to create new optical phase states and highly efficient devices not accessible by periodic metasurfaces.[9,11] These findings underpin that embracing structural disorder could lead to metasurfaces

K. Tanaka, A. Fitriana, D. Pidgayko, I. Staude
Abbe Center of Photonics
Friedrich-Schiller-University Jena
Albert-Einstein-Straße 6, 07745 Jena, Germany
E-mail: katsuya.tanaka@uni-jena.de

K. Tanaka, A. Fitriana, D. Pidgayko, I. Staude
Institute of Solid State Physics
Friedrich-Schiller-University Jena
Helmholtzweg 5, 07743 Jena, Germany

K. Tanaka, T. Pertsch, C. Rockstuhl, I. Staude
Max Planck School of Photonics
Hans-Knöll-Straße 1, 07745 Jena, Germany

A. Rahimzadegan
Sustainable and Bio-inspired Materials
Max Planck Institute of Colloids and Interfaces
14476 Potsdam, Germany

D. Arslan, T. Pertsch
Fraunhofer Institute for Applied Optics and Precision Engineering IOF
Albert-Einstein-Straße 7, 07745 Jena, Germany

S. Fasold, M. Steinert, T. Pertsch, M. Decker
Institute of Applied Physics
Abbe Center of Photonics
Friedrich Schiller University Jena
Albert-Einstein-Straße 15, 07745 Jena, Germany

C. Rockstuhl
Institute of Theoretical Solid State Physics
Karlsruhe Institute of Technology
76131 Karlsruhe, Germany

C. Rockstuhl
Institute of Nanotechnology
Karlsruhe Institute of Technology
76131 Karlsruhe, Germany

The ORCID identification number(s) for the author(s) of this article can be found under https://doi.org/10.1002/adom.202402898

DOI: 10.1002/adom.202402898

with novel and robust optical properties. Building on this understanding, our research focuses on harnessing orientational disorder in chiral nanostructures to achieve a chiroptical response that is largely independent of the incident angle. The orientational disorder is, therefore, vital to observing purely chiroptical effects such as circular dichroism (CD) and optical activity (OA). The orientational disorder in chiral metasurfaces refers to the deliberate randomization of the rotational orientation of individual meta-atoms around their vertical axis, within a specified angular range. This randomness modifies the local symmetry of the metasurface while preserving the overall periodic arrangement, introducing quasi-continuous rotational symmetry. Such symmetry effectively acts as an infinitely large supercell, suppressing birefringent effects and maintaining orthogonal circular eigenpolarizations. Here, "eigenpolarizations" or "polarization eigenvectors" refers to the polarization eigenvectors of the Jones matrix of the disordered metasurface. As a result, the structure exhibits robust and consistent chiroptical responses across a broad spectral range. In this work, we refer to "purely chiral" as the ability of a metasurface to exhibit circular eigenpolarizations, resulting in highly selective interaction with left- (LCP) and right-handed circularly polarized (RCP) light while linear birefringence is strongly suppressed. This property is quantified using the "LCP/RCP purity" values, which measure the extent to which the transmitted light retains its original circular polarization state. These purity values provide a robust metric for evaluating the chiral response of metasurfaces across various conditions. This behavior parallels the optical response observed in natural chiral solutions, such as randomly oriented molecules in solution, highlighting the analogy between biological and metasurface-based systems. In natural systems, such as randomly oriented chiral molecules in solution, pure chiroptical effects, including circular dichroism and optical activity, arise from circular eigenpolarizations that are robust against variations in molecular orientation. We aim to replicate these properties in metasurfaces by introducing controlled orientational disorder in chiral dielectric nanostructures. Many research groups have created artificial chiral nanostructures that surpass the chiroptical functionalities of natural molecules.[12–17] However, these designs typically rely on periodically arranged nanoarrays with ordered orientations, resulting in a strong dependence of man-made chiral structures on the polarization axis of the input beam.[18–20] Planar chiral metasurfaces can exhibit strong chiro-optical effects such as circular polarization conversion and asymmetric transmission of circular polarizations.[21,22] While planar designs leverage extrinsic effects to achieve chirality, bilayer (3D) chiral metasurfaces provide true geometrical chirality due to symmetry breaking in all spatial dimensions. This intrinsic chirality enables bilayer metasurfaces to achieve intrinsic circular eigenpolarizations, offering maximum flexibility for tailoring chiral optical responses.[16,23,24] Moreover, most chiral metamaterials investigated so far do not exhibit pure chiroptical responses, as achieving circular eigenpolarizations typically requires at least threefold rotational symmetry in the arrangement of the chiral unit cell.[16,18–20,23,25] Although circular eigenpolarizations are commonly associated with at least threefold rotational symmetry, recent work has shown that metasurfaces with no rotational symmetry can achieve pure chiroptical responses under normal incidence through tailored symmetry-breaking mechanisms.[26] While it is possible to restore symmetry by arranging rotated elements in a supercell,[16,23] this approach typically requires larger unit cells, leading to unwanted diffractive features. In our previous work,[23] we demonstrated that circular dichroism with pure circular eigenpolarizations could be achieved using C_4 rotationally symmetric dielectric chiral structures. While these metasurfaces exhibited strong and pure chiroptical responses due to the excitation of a chiral super-mode, our study was limited to normal incident light only. However, periodic chiral structures generally exhibit strong dependence on the incident angle, complicating the maintenance of a consistent chiral response across different viewing angles. In contrast, this angular dependence can be intentionally exploited through extrinsic chirality, where a chiral response is obtained even from otherwise achiral structures.[27,28] Our current study addresses these limitations by introducing orientational disorder in the chiral elements ("meta-atoms") composing the metasurface. Previously, we already showed for chiral plasmonic metasurfaces that the orientational disorder of chiral twisted gold dimers could effectively create an infinitely large supercell with quasi-continuous rotational symmetry, suppressing diffractive features and enabling operation across a broad spectral range without linear birefringence.[29] However, the use of lossy plasmonic metals in that study limited the resonance quality at optical frequencies, making it difficult to separate the additional effect of disorder-induced scattering losses on the overall response. Moreover, the behavior of the structure at different incidence angles was not studied.

2. Results and Discussion

Here, we experimentally and numerically investigate the chiroptical response resulting from rotational disorder in chiral bilayer metasurfaces composed of extremely low-absorbing dielectric nanoresonators. Remarkably, we observed nearly circular eigenpolarizations that remained largely independent of the incident angle within the studied range—a behavior resembling that of randomly oriented chiral molecules in solution, such as sugars and amino acids. Importantly, comparison with the optical response of the corresponding ordered metasurfaces, where the low absorption losses in the dielectric material facilitate strong and sharp dispersive resonances, allows us to clearly identify the impact of the disorder on the resonant response. Our findings underscore the potential of tailored disorder to enhance the robustness of the chiroptical response of resonant metasurfaces and suggest new possibilities for designing high-efficiency, compact optical components, such as circular polarizers, beam splitters, and polarization shapers.

To explore the chiroptical response enabled by orientational disorder, we designed a chiral bilayer dielectric metasurface composed of silicon nanocuboids supporting Mie-type resonances in the near-infrared spectral range (see **Figure 1a** for a conceptual image). As shown in Figure 1b, the basic building block consists of two silicon nanocuboids. The two nanocuboids are stacked vertically with a separation distance of $s = 255$ nm along the z-axis. The top nanocuboid has dimensions $a = 371$ nm, $b = 403$ nm, and $c = 142$ nm, while the bottom nanocuboid has dimensions $d = 371$ nm, $e = 403$ nm, and $f = 142$ nm. These nanocuboids are rotated relative to each other by $\pm 60°$ in the x-y plane, resulting in left-handed (LH) and right-handed (RH) chiral

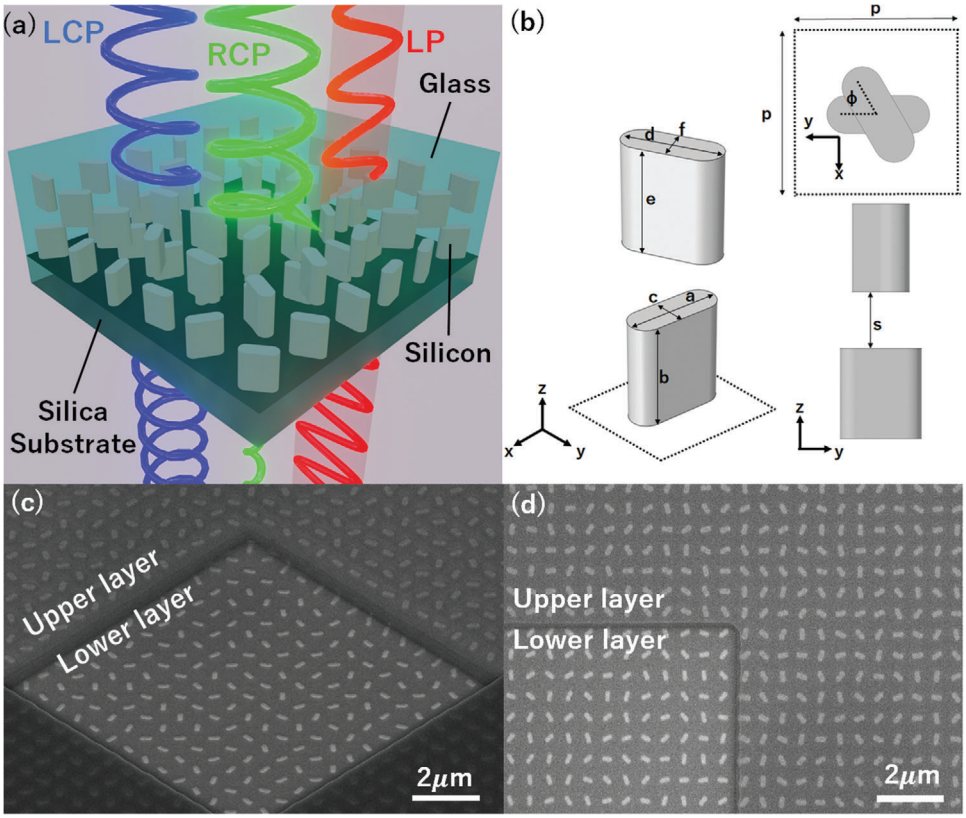

Figure 1. a) Conceptual image of chiro-optical effects. In particular, the presence of a circular dichroism and optical activity observed in disordered chiral bilayer all-dielectric metasurfaces is highlighted. b) Configuration of the individual chiral building block. c) Oblique-view and d) top-view SEM images of the fabricated bilayer metasurfaces, with both layers revealed by FIB milling.

structures, as depicted in Figure 1b. The geometrical parameters of the metasurface were chosen with consideration for robustness against fabrication errors, drawing on insights from earlier simulations and experimental findings on related structures.[23] The angle $\phi = \pm 60°$ was selected based on prior simulations of C_2-symmetric structures,[23] which indicated that this angle provides a practical balance between maintaining strong optical responses and achieving the symmetry-breaking necessary for chirality. The entire bilayer structure is embedded in a glass matrix and placed on a fused silica substrate. The homogeneous embedding prevents substrate-induced asymmetries.To induce orientational disorder, each building block was randomly rotated by an angle between 0° and 360° around the z-axis while maintaining a periodic arrangement with a center-to-center structural spacing between neighboring dimers $p = 700$ nm.The chiral bilayer metasurfaces were fabricated using a two-step electron beam lithography (EBL) process.[23] In the first step, the lower layer of nanocuboids was patterned on a fused silica substrate. Following the development, a thin spacer layer of glass was deposited. The second EBL process was then performed to align and stack the upper layer of nanocuboids on top of the spacer layer, completing the bilayer structure. While keeping most of the metasurface area (500 μm × 500 μm) intact for optical characterization, a small section of the final structure was revealed by focused ion beam (FIB) milling to obtain scanning electron microscopy (SEM) images of both layers together for structural verification (Figure 1c,d).

Polarization-resolved linear-optical spectroscopy measurements were conducted to investigate the chiroptical properties of the fabricated metasurfaces. In the first step, both enantiomers of the metasurfaces were illuminated with incoherent broadband LCP and RCP light under normal incidence. The transmission spectra were recorded for both LCP and RCP outputs, allowing us to observe circular dichroism and assess the purity of circular eigenpolarizations.

Figure 2a–d shows the transmission spectra of left- and right-handed chiral metasurfaces for circularly polarized incident light. The notation $T_{\mathrm{LCP/RCP} \rightarrow \mathrm{LCP/RCP}}$ denotes the transmittance when LCP or RCP light is used as input, with the same or opposite polarization detected at the output, respectively. Specifically, $T_{\mathrm{LCP} \rightarrow \mathrm{LCP}}$ and $T_{\mathrm{RCP} \rightarrow \mathrm{RCP}}$ represent polarization-conserving transmittance, while $T_{\mathrm{RCP} \rightarrow \mathrm{LCP}}$ and $T_{\mathrm{LCP} \rightarrow \mathrm{RCP}}$ indicate polarization conversion. The measured spectra (Figure 2a,b) reveal distinct differences in transmittance between LCP and RCP illumination, with these differences reversing between the LH and RH structures. This reversal confirms the strong chiral nature of the metasurfaces, as each enantiomer selectively interacts with its corresponding circular polarization. Notably, a pronounced dip is observed around 1.41 μm for RCP to RCP in the LH structure (a) and LCP to LCP in the RH structure (b). These features can be attributed to the excitation of Mie-type magnetic dipole resonances within the silicon nanocuboids, which are excitable only by a specific circular polarization, as discussed in Ref. [23] for periodic

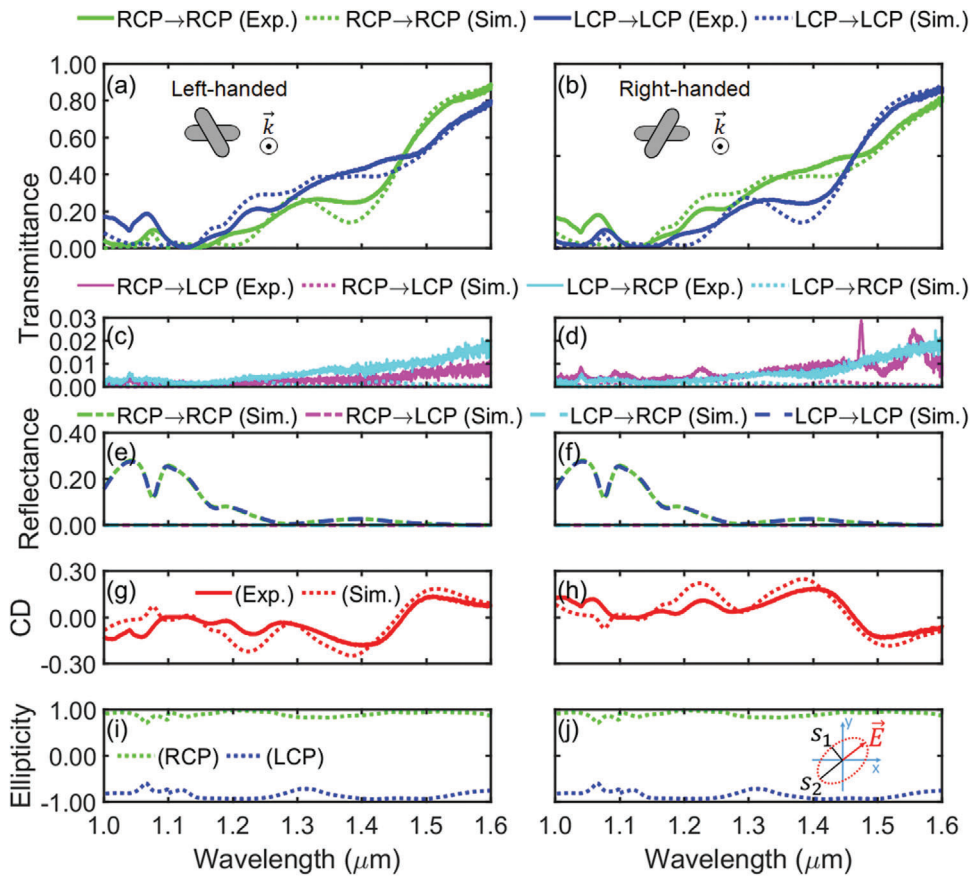

Figure 2. Experimentally measured and simulated transmission spectra of left- (left column) and right-handed (right column) chiral metasurfaces under illumination with circularly polarized light. a,b) show the polarization-conserving transmittance (LCP → LCP, RCP → RCP), c,d) the polarization conversion (RCP → LCP, LCP → RCP), e,f) the reflectance and g,h) the CD. The calculated ellipticity of the eigenpolarizations is displayed in i,j), indicating the high purity of the metasurfaces' chiral response.

metasurfaces. Crucially, the polarization conversion (RCP → LCP and LCP → RCP) remains minimal (below 3%) across the entire considered spectral range, as shown in Figure 2c,d. The suppressed polarization conversion suggests that the eigenpolarizations are predominantly circular, and the optical response is governed by circular dichroism.[16] The simulated reflection spectra in Figure 2e,f confirm that reflection remains low across the spectral range, indicating that the transmission suppression, such as at 1.1 m, arises primarily from scattering. This is likely due to homogenized resonances, where rotational disorder broadens the resonant features, such as electric and magnetic dipole modes.[23] The broadening and attenuation of these resonances result in a redistribution of light into non-forward directions, a behavior characteristic of disordered systems.[11] CD can be defined by considering the co-polarized and cross-polarized transmission components for RCP and LCP light according to:

$$CD = \frac{(T_{\mathrm{RCP}\to\mathrm{RCP}} + T_{\mathrm{RCP}\to\mathrm{LCP}}) - (T_{\mathrm{LCP}\to\mathrm{LCP}} + T_{\mathrm{LCP}\to\mathrm{RCP}})}{(T_{\mathrm{RCP}\to\mathrm{RCP}} + T_{\mathrm{LCP}\to\mathrm{RCP}}) + (T_{\mathrm{LCP}\to\mathrm{LCP}} + T_{\mathrm{RCP}\to\mathrm{LCP}})} \quad (1)$$

The observed highly pure CD directly results from the high rotational symmetry introduced by the orientational disorder, which effectively suppresses linear birefringence and ensures consistent performance across a broad wavelength range. The maximum circular dichroism, ∓ 0.18 at 1.41 μm (Figure 2g,h), validates the metasurface design and compares favorably with previous studies on disordered chiral plasmonic metasurfaces.[29] To complement the experimental results, we performed detailed numerical simulations using a T-matrix-based multiple scattering approach. Unlike traditional large-scale finite-difference time-domain (FDTD) simulations, which are often used to model disordered metamaterials,[30,31] the T-matrix-based approach provides a more efficient framework for accounting for the complex electromagnetic interactions specific to disordered systems. Moreover, this method offers valuable insights into the behavior of chiral eigenpolarizations and the nature of the associated resonances, which would be difficult to capture with FDTD alone. Specifically, here we apply the local-coordinate T-matrix method[9,32] to capture the effects of rotational disorder in chiral bilayer dielectric metasurfaces.

In the first step of our simulations, we calculate the T-matrix of a single nanocuboid with rounded vertical edges (rounding radius 71 nm, see Figure 1b) embedded in a homogenous silica embedding. We assumed that both nanocuboids in the two layers have the same size parameters. We used the finite element solver JCMsuite to calculate the T-matrix of the nanocuboid. In

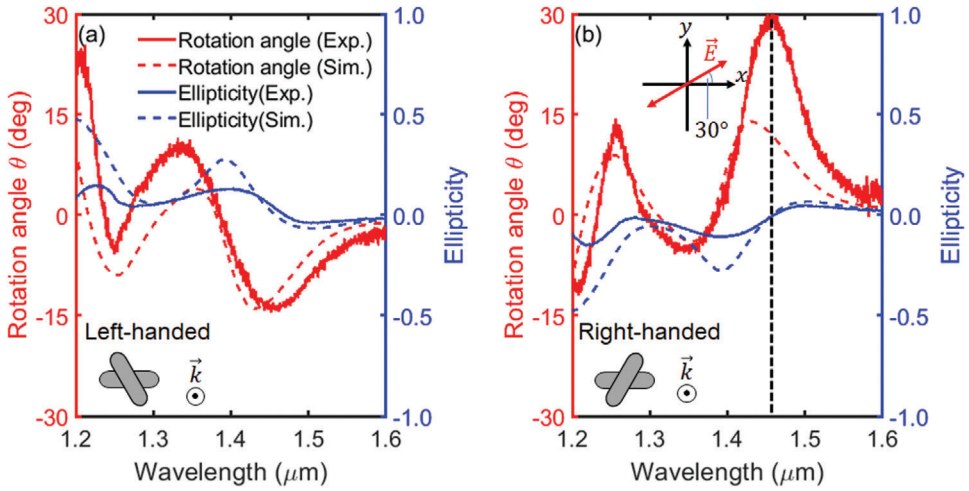

Figure 3. a,b) Rotation angle of the major polarization axis and ellipticity of *x*-polarized incident light after transmission through the left- (a) and right- (b) handed disordered chiral metasurfaces.

the solver, the nanocuboid is excited with vector spherical harmonics of different total angular momentum, orbital angular momentum, and parity, and the scattered field is calculated across a closed surface circumscribing the nanocuboid. These scattered fields are projected into vector spherical harmonics to extract all individual components of the T-matrix characterizing an individual nanocuboid.[33]

In the second step, we study the optical response from a sufficiently large finite-sized disordered metasurface. The finite metasurface consists of 7 × 7 unit cells. Each unit cell contains two nanocuboids forming a pair. Within each pair, the two nanocuboids are oriented at 60 degrees to each other, while each pair is given a random orientation. Using a T-matrix-based multiple scattering code,[34] we then calculate the scattered light from the ensemble of particles under illumination with normal-incidence plane-wave. The algorithm is highly efficient as each cuboid is represented by its previously retrieved T-matrix only, and the entire algorithm boils down to a matrix-vector product. The T-matrix of the considered cuboid is relatively small, and a quadrupolar approximation is sufficient to reach convergent results. We then collect the scattered field in a plane close to the second layer in transmission and parallel to the metasurface. The spatial average of the scattered field plus the incident field results in the zero-order transmission. To compensate for the fact that transmission is only calculated for a specific implementation of the disorder, we repeated the calculation with different random orientations 20 times and took the overall average. That procedure allows us to predict the transmission on computational grounds highly accurate.

The simulated transmittance, reflectance and CD spectra are plotted alongside the experimental curves in Figure 2a–h. Excellent agreement is achieved regarding the number and spectral positions of the observed resonances, underscoring the adequacy of the numerical model employed. However, some deviations are observed, and the experimental results show less pronounced resonances than the simulations. These discrepancies are likely due to unavoidable fabrication inaccuracies, including particle poly dispersity and alignment errors, surface roughness, asymmetries, and minor material variations. These aspects are not taken into account in the idealized theoretical description.

Importantly, while only intensities are recorded in our experiment, the simulations yield the full complex transmittance of the investigated metasurfaces. Access to the simulated complex amplitudes enables us to calculate the ellipticity of the eigenpolarizations of our structures. The corresponding results are shown in Figure 2i,j. The ellipticity of the eigenpolarizations, represented as the ratio of the minor (s_1) to major (s_2) axes of the polarization ellipse ($e = s_2/s_1$), quantitatively describes the deviation from linear polarization. For the metasurfaces investigated, the ellipticity consistently approaches ±1 across the spectral range, indicating nearly perfect circular polarization eigenvectors, independent of the wavelength.

Next, for a quantitative evaluation of the optical activity of the chiral disordered metasurfaces, we measured and numerically simulated the rotation angle of the major polarization axis of linearly polarized light after passing through the structures. To this end, the rotating quarter-waveplate method was employed.[35] **Figure** 3a,b shows the rotation angle for linearly *x*-polarized light after passing through the left- and right-handed chiral structures, respectively, alongside the measured output ellipticity. At 1.46 μm, the RH metasurface achieves a maximum experimental optical rotation θ of 30 degrees, while the LH metasurface reaches a minimum of –15 degrees. In both cases, the output polarization remains nearly linear, with the ellipticity $e < 0.15$ for the RH structure and $e < 0.13$ for the LH structure. Despite the scattering losses introduced through rotational disorder, the observed values for the optical activity are comparable to those observed for plasmonic twisted split-ring resonator structures.[16] The experimentally observed performance differences between the two enantiomers can be attributed to fabrication imperfections, particularly related to the alignment of the two layers, which showed deviations on the scale of 10 nm, as observed in the SEM images.

Again, a good qualitative agreement is obtained with corresponding simulated results. However, quantitatively, the experimental results consistently show a smaller ellipticity of the output polarization, consistent with the slightly smaller CD observed in

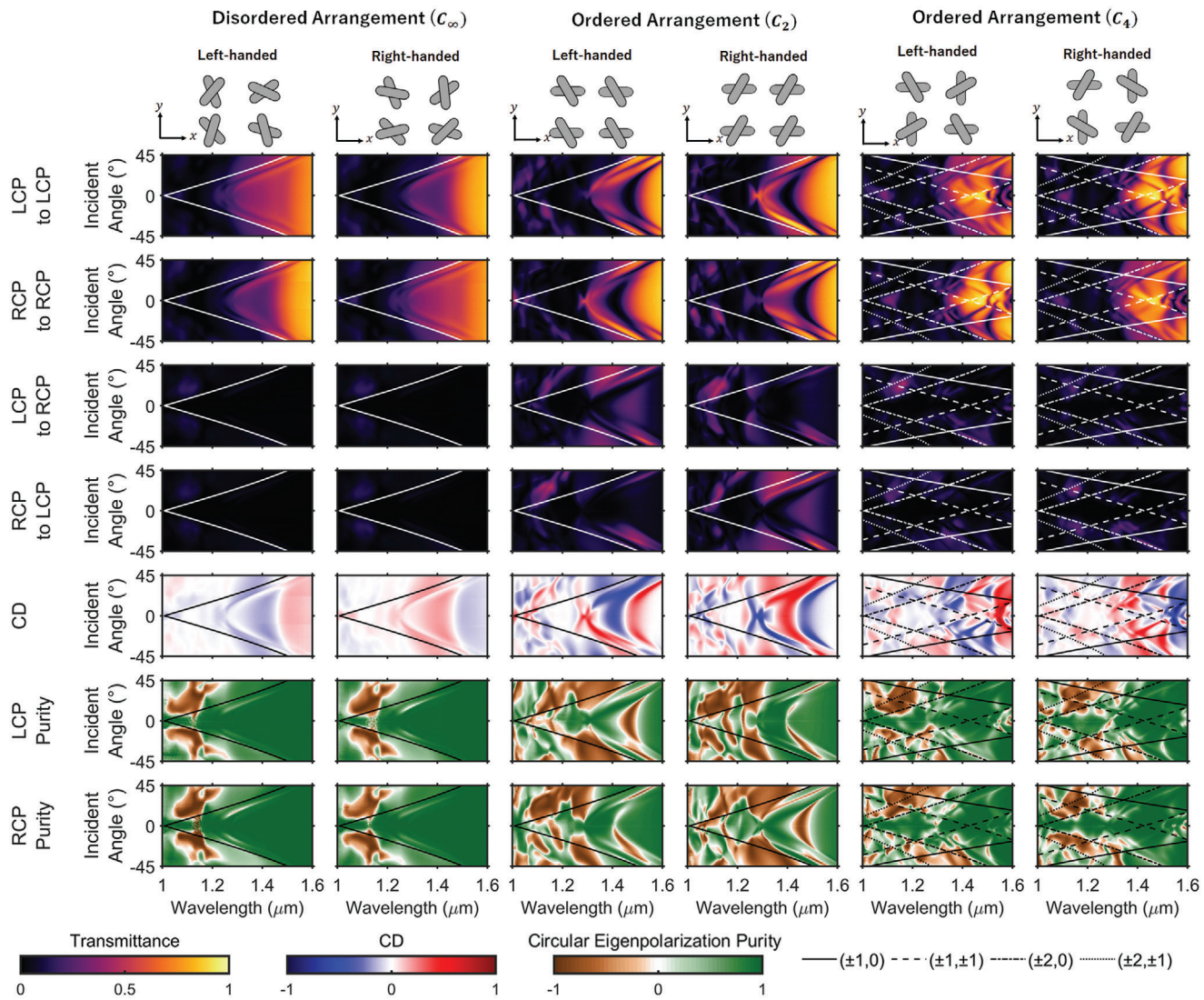

Figure 4. Angle-dependent response of chiral metasurfaces in experiment. Rows one to four show the transmission spectra (LCP to LCP, RCP to RCP, LCP to RCP, and RCP to LCP channels) and row five CD as functions of the incident angle for both disordered (left panel) and ordered (middle and right panels) configurations of LH and RH chiral metasurfaces. The white dashed lines indicate the boundaries for the first-order diffraction condition. The bottom row displays the RCP/LCP purities.

the experiment (see Figure 2). Additionally, for the RH metasurface, the maximum optical rotation is larger in experiments than in simulations, hinting toward deviations in the exact phase value imposed by the coupled Mie resonances at given wavelengths. Such deviations can originate from slight differences in the geometrical parameters of the individual nanocuboids realized in the experimental structure compared to theoretically assumed values.

Finally, we investigated the optical response of the disordered chiral metasurfaces under oblique incidence and compared it to corresponding ordered, fully periodic structures. Both C_2 symmetric and C_4 symmetric ordered arrangements were considered as reference structures, noting that only the C_4 symmetric structure can support circular eigenpolarizations under normal incidence.[16] For both disordered (C_∞) and ordered (C_2 and C_4) configurations, both enantiomers were fabricated and analyzed.

Corresponding results are summarized in **Figure 4**. Note that the oblique incidence was along the x-direction, as indicated in the figure. The first two rows show the measured co-polarized transmittance, and the next two rows show the cross-polarized transmittance. The CD is plotted in the fifth row. For wavelengths $\lambda > (1.44 + \sin\theta)p$, where p is the period of the underlying square lattice structure and 1.44 the average refractive index of the surrounding silicon dioxide, the structure is non-diffractive. The solid white lines in the images for the C_∞ and C_2 structures indicate the onset of diffraction, shown for $p = 0.7$ μm. For the C_4 symmetric structures with $p = 1.4$ μm, the onset of multiple 2D diffraction orders, such as (±1, 0), (±1, ±1), (±2, 0), and (±2, ±1), can be observed within the considered spectral and incident-angle range. These boundaries are derived using the standard 2D grating diffraction theory.[36,37] As already observed for normal incidence, in all configurations, the angularly resolved

transmission of the LH structure under LCP incidence closely mirrors that of the RH structure under RCP incidence. Such a resemblance is expected from the chiral symmetry of the structure, which further underpins the high quality of our fabricated structures.

Comparing the angularly resolved spectra between the different configurations, it is immediately apparent that the optical response for the disordered metasurface is much smoother than for the ordered arrangements, showing a weaker dependence on incidence angle and wavelength. All configurations exhibit Mie resonances. However, while for the ordered configurations a strong interaction of these Mie resonances with the respective diffractive (lattice) modes is observed, resulting in a strong angular dispersion of their associated spectral features, this coupling appears to be suppressed for the disordered configuration.

As a result, for the disordered arrangement, the resonance dips observed at 1.41 μm in the LCP → LCP (RCP → RCP) channel for the RH (LH) structure persist within a comparably large incident angle range of approximately –20 to 20 degrees before the response becomes dominated by a dispersive feature tracing out the onset of diffraction from the underlying square lattice. In contrast, for the C_2 symmetric structure, the corresponding resonance dip, while being more pronounced, exhibits a strong redshift with increasing angle. For the C_4 symmetric structure, the large supercell supports additional diffraction orders. These additional diffraction orders result in a complicated dispersive behavior of the resonant metasurface response. Important differences between the configurations are furthermore observed in the polarization conversion channels. For the disordered arrangement, the conversions remain negligible throughout the considered wavelength and angle range. That observation shows that the high purity of the circularly polarized eigenpolarizations is well preserved, even at high angles of incidence. The observed high purity of circular eigenpolarizations in the disordered metasurface can be attributed to the quasi-continuous rotational symmetry introduced by the orientational disorder. Similar to the findings by Fasold et al.,[29] this disorder eliminates linear birefringence while preserving circular dichroism and optical activity, leading to a globally isotropic chiroptical response. This approach contrasts with ordered metasurfaces, which rely on explicit rotational symmetry and exhibit angle-sensitive responses. This behavior resembles, to some degree, that of natural chiral molecules, such as sugars and amino acids, which maintain polarization purity irrespective of orientation. Conversely, the C_2 symmetric structure shows strong polarization conversion across various areas of the investigated parameter space, including for normal incidence. As noted above, this is expected from the lack of at least threefold rotational symmetry, resulting in non-circular eigenpolarizations for this structure. For the C_4 symmetry case, polarization conversion vanishes at normal incidence, as previously discussed in ref. [23]. However, polarization conversion starts playing a significant role for oblique incidence, indicating that the structure cannot sustain circular eigenpolarizations under these conditions. Such a finding is quantitatively confirmed by the maximum conversion values observed within the dominant diffraction cones, spanned by the (± 1, 0) lines for C_∞ and C_2, and by the (± 2, 0) lines for C_4: 0.08 for C_∞, 0.71 for C_2, and 0.41 for C_4. The higher conversion values for C_2 and C_4 indicate a significant deviation from ideal circular eigenpolarizations, emphasizing the structure's sensitivity to symmetry breaking under oblique incidence.

The described features of the measured angle-resolved transmittance for the three configurations directly translate to the properties of the respective CD. As such, CD is generally weaker but less dispersive for the disordered case than for its ordered counterparts. Moreover, for both the C_2 and C_4 symmetric structures, the presence of elliptical output polarization due to polarization conversion limits their potential for practical applications. To further explore the described trade-off between the strength of the resonance response and undesired conversion, we define new figures of merit denoted LCP/RCP purity, respectively, as follows:

$$\text{LCP purity} = \frac{T_{\text{LCP}\to\text{LCP}} - T_{\text{LCP}\to\text{RCP}}}{T_{\text{LCP}\to\text{LCP}} + T_{\text{LCP}\to\text{RCP}}}$$
$$\text{RCP purity} = \frac{T_{\text{RCP}\to\text{RCP}} - T_{\text{RCP}\to\text{LCP}}}{T_{\text{RCP}\to\text{RCP}} + T_{\text{RCP}\to\text{LCP}}} \quad (2)$$

These purity values quantify how much of the transmitted light for a given circular input polarization (LCP or RCP) is converted into the orthogonal polarization. A purity of 1 indicates that none of the transmitted light undergoes a polarization conversion, 0 indicates equal transmission and conversion, and –1 indicates complete conversion of the transmitted light with no transmission of the original polarization. Importantly, this quantity corrects for the influence of the total transmitted intensity.

In terms of RCP/LCP purity, the disordered case shows outstanding performance, with both LCP and RCP purity remaining nearly 1 over a large parameter space, especially in the non-diffractive regime where CD effects are most prominent. These findings indicate that the system can maintain highly pure circular states upon transmission, even under large incidence angles. Conversely, in the C_2 case, the purity values show fast fluctuations between –1 and 1 as a function of both wavelength and incident angle. Finally, in the C_4 case, the circular eigenpolarization purity approaches 1 near normal incidence. However, as the incident angle increases, the purity decreases due to the effective breaking of the C_4 symmetry by the tilted excitation. As such, none of the two ordered configurations can provide a pure and angle-tolerant chiroptical response.

3. Conclusion

In conclusion, we successfully demonstrated a robust chiroptical response in chiral bilayer square lattice of dielectric metasurfaces with orientational disorder, characterized by significant CD and OA. Experimentally, the CD reached 0.18 (RH structure) and –0.18 (LH structure), while the OA measured 30 degrees (RH structure) and –15 degrees (LH structure). These results surpass those observed in previously studied chiral plasmonic metasurfaces, offering advantages in terms of lower absorption and broader bandwidths due to the use of dielectric materials.While prior studies have achieved maximal polarization purity using bound states in the continuum[21,26,38,39] or explored other mechanisms such as spin-preservation[40] and arbitrary polarization manipulation,[41] their chiroptical responses are often restricted to specific wavelengths and narrow

angular ranges, unlike the broadband and angle-tolerant properties demonstrated in this work. Future enhancement of the circular dichroism of disordered chiral metasurfaces could be achieved by further optimizing the nanoresonator design and nanofabrication process, tailoring the optical properties, particularly the losses, of the constituent materials of the metasurface toward the critical coupling condition,[38] and engineering the statistical properties of disorder. introducing degrees of short-range order could enhance localized chiral interactions while maintaining global isotropy. In particular, introducing degrees of short-range order could enhance localized chiral interactions while maintaining global isotropy. Importantly, the implemented rotational disorder strongly enhances the robustness of the pure circular eigenpolarizations to the incident angle. This robustness in the angle-dependent response is accommodated with a weakening of dispersive diffractive features and their influence on the overall response of the disordered metasurface. Qualitatively, we can understand this behavior in analogy to natural media hosting chiral molecules in random orientations. Note, however, that in our case, the orientation of the chiral dimers composing the metasurface is only randomized concerning one axis. From an application perspective, chiral metasurfaces show significant potential for compact and versatile optical components such as circular polarizers, beam splitters, and polarization shapers. For such components, the angular dependence of the chiral response can play a crucial role. Our work clearly highlights the opportunities offered by disordered configurations of chiral metasurfaces regarding a robust angular performance, which is favorable whenever a careful alignment of components cannot be guaranteed. At the same time, while the ordered arrangements are much less robust, their strong resonant and highly dispersive response may enable carefully tailored complex responses in different functional regimes. Future work may explore varying degrees of disorder and scalability, opening avenues for practical applications and further innovation in metasurface design.

4. Experimental Section

The experimental setup for optical characterization follows the methodology described in ref. [23], with detailed component specifications provided here for reproducibility. The broadband light source used was a halogen lamp (Thorlabs, Model SLS301, wavelength range: 360–3800 nm). The light was collimated into a parallel beam using a collimator (Thorlabs, Model RC02, focal length: 7 mm). Circularly polarized input light was generated using a linear polarizer (Thorlabs, Model LPNIR100, wavelength range: 650–2000 nm) and a quarter-wave plate (Bernard Halle Nachfl, Model RSU 2.4.10, wavelength range: 600–2700 nm). The transmitted light was collected by an optical system with a low NA (0.044) to suppress contributions from scattered light. The collection optics included lenses (Thorlabs, Models LA1131 and LA1464) and field stops (Thorlabs, Model ID8/M) to ensure precise light collection. The objective lens (Thorlabs, Model RMS4X, magnification: 4×) was aligned coaxially with the incident beam to focus the transmitted light onto into the fiber-coupling system while maintaining the specified NA, limiting the acceptance angle to approximately 2.5°. This configuration ensured that only the zeroth-order diffraction was collected, minimizing scattering light contributions by restricting the collection to a narrow angular range. The transmitted light was then directed to an optical spectrum analyzer (Yokogawa, Model AQ6370B, wavelength range: 600–1700 nm) via a fiber-coupled input (Thorlabs, M43L01) for spectral analysis.

Acknowledgements

This work was funded by the Deutsche Forschungsgemeinschaft (DFG, German Research Foundation), Project-IDs: 437527638 – IRTG 2675 (Meta-Active), STA 1426/1-2, and STA 1426/2-1. This project was made possible by funding from the Carl Zeiss Foundation. The authors thank A. Ihring, H. Schmidt, D. Voigt, T. Kaesebier, and M. Banasch for their assistance in sample fabrication. The authors sincerely thank Xavier Garcia-Santiago for their support in JCMsuite simulations. Katsuya Tanaka is part of the Max Planck School of Photonics supported by BMBF, Max Planck Society, and Fraunhofer Society. The authors were grateful to the company JCMwave for their free provision of the FEM Maxwell solver JCMsuite.

Open access funding enabled and organized by Projekt DEAL.

Conflict of Interest

The authors declare no conflict of interest.

Data Availability Statement

The data that support the findings of this study are available from the corresponding author upon reasonable request.

Keywords

all-dielectric nanophotonics, chirality, disorder, metasurfaces, mie resonances, silicon

Received: October 25, 2024
Revised: December 28, 2024
Published online:

[1] N. Yu, F. Capasso, *Nat. Mater.* **2014**, *13*, 139.
[2] A. I. Kuznetsov, A. E. Miroshnichenko, M. L. Brongersma, Y. S. Kivshar, B. Luk'yanchuk, *Science* **2016**, *354*, 6314.
[3] S. A. Schulz, R. F. Oulton, M. Kenney, A. Alú, I. Staude, A. Bashiri, Z. Fedorova, R. Kolkowski, A. F. Koenderink, X. Xiao, J. Yang, W. J. Peveler, A. W. Clark, G. Perrakis, A. C. Tasolamprou, M. Kafesaki, A. Zaleska, W. Dickson, D. Richards, A. Zayats, H. Ren, Y. Kivshar, S. Maier, X. Chen, M. A. Ansari, Y. Gan, A. Alexeev, T. F. Krauss, A. Di Falco, S. D. Gennaro, et al., *Appl. Phys. Lett.* **2024**, *124*, 26.
[4] M. V. Rybin, Y. Kivshar, *npj Nanophotonics* **2024**, *1*, 1.
[5] V. E. Babicheva, A. B. Evlyukhin, *Adv. Opt. Photonics* **2024**, *16*, 539.
[6] A. A. Zharov, I. V. Shadrivov, Y. S. Kivshar, *J. Appl. Phys.* **2005**, *97*, 113906.
[7] S. S. Kruk, C. Helgert, M. Decker, I. Staude, C. Menzel, C. Etrich, C. Rockstuhl, C. Jagadish, T. Pertsch, D. N. Neshev, Y. S. Kivshar, *Phys. Rev. B* **2013**, *88*, 20.
[8] D. Veksler, E. Maguid, N. Shitrit, D. Ozeri, V. Kleiner, E. Hasman, *ACS Photonics* **2015**, *2*, 661.
[9] A. Rahimzadegan, D. Arslan, R. Suryadharma, S. Fasold, M. Falkner, T. Pertsch, I. Staude, C. Rockstuhl, *Phys. Rev. Lett.* **2019**, *122*, 1.
[10] M. Jang, Y. Horie, A. Shibukawa, J. Brake, Y. Liu, S. M. Kamali, A. Arbabi, H. Ruan, A. Faraon, C. Yang, *Nat. Photonics* **2018**, *12*, 84.
[11] D. Arslan, A. Rahimzadegan, S. Fasold, M. Falkner, W. Zhou, M. Kroychuk, C. Rockstuhl, T. Pertsch, I. Staude, *Adv. Mater.* **2021**, *34*, 5.
[12] V. A. Fedotov, A. S. Schwanecke, N. I. Zheludev, V. V. Khardikov, S. L. Prosvirnin, *Nano Lett.* **2007**, *7*, 1996.
[13] J. K. Gansel, M. Thiel, M. S. Rill, M. Decker, K. Bade, V. Saile, G. von Freymann, S. Linden, M. Wegener, *Science* **2009**, *325*, 1513.

[14] Y. Zhao, A. N. Askarpour, L. Sun, J. Shi, X. Li, A. Alù, *Nat. Commun.* **2017**, *8*, 14180.
[15] M. Decker, M. Ruther, C. E. Kriegler, J. Zhou, C. M. Soukoulis, S. Linden, M. Wegener, *Opt. Lett.* **2009**, *34*, 2501.
[16] M. Decker, R. Zhao, C. M. Soukoulis, S. Linden, M. Wegener, *Opt. Lett.* **2010**, *35*, 1593.
[17] M. Hentschel, M. Schäferling, T. Weiss, N. Liu, H. Giessen, *Nano Lett.* **2012**, *12*, 2542.
[18] J. Kaschke, J. K. Gansel, M. Wegener, *Opt. Express* **2012**, *20*, 26012.
[19] I. Fernandez-Corbaton, *Opt. Express* **2013**, *21*, 29885.
[20] I. Fernandez-Corbaton, M. Fruhnert, C. Rockstuhl, *ACS Photonics* **2015**, *2*, 376.
[21] T. Shi, Z.-L. Deng, G. Geng, X. Zeng, Y. Zeng, G. Hu, A. Overvig, J. Li, C.-W. Qiu, A. Alú, Y. S. Kivshar, X. Li, *Nat. Commun.* **2022**, *13*, 1.
[22] X. Wang, H. Hao, X. He, P. Xie, J. Liu, J. Tan, H. Li, H. Wang, P. Genevet, Y. Luo, X. Ding, G. Hu, *Nat. Rev. Electr. Eng.* **2024**, *1*, 391.
[23] K. Tanaka, D. Arslan, S. Fasold, M. Steinert, J. Sautter, M. Falkner, T. Pertsch, M. Decker, I. Staude, *ACS Nano* **2020**, *14*, 15926.
[24] N. Liu, H. Liu, S. Zhu, H. Giessen, *Nat. Photonics* **2009**, *3*, 157.
[25] J. Kaschke, M. Blome, S. Burger, M. Wegener, *Opt. Express* **2014**, *22*, 19936.
[26] L. Kühner, F. J. Wendisch, A. A. Antonov, J. Bürger, L. Hüttenhofer, L. de S. Menezes, S. A. Maier, M. V. Gorkunov, Y. Kivshar, A. Tittl, *Light: Sci. Appl.* **2023**, *12*, 1.
[27] Y. Zhao, M. Belkin, A. Alú, *Nat. Commun.* **2012**, *3*, 1.
[28] T. Cao, C. Wei, L. Mao, Y. Li, *Sci. Rep.* **2014**, *4*, 1.
[29] S. Fasold, S. Linß, T. Kawde, M. Falkner, M. Decker, T. Pertsch, I. Staude, *ACS Photonics* **2018**, *5*, 1773.
[30] K. Tsuruta, S. Nagai, R. Umeda, T. Kurose, N. Maetani, *MRS Proc.* **2009**, *1223*.
[31] C. Kang, C. Park, M. Lee, J. Kang, M. S. Jang, H. Chung, *Nanophotonics* **2024**, *13*, 3765.
[32] R. N. S. Suryadharma, M. Fruhnert, I. Fernandez-Corbaton, C. Rockstuhl, *Phys. Rev. B* **2017**, *96*, 045406.
[33] A. Rahimzadegan, T. D. Karamanos, R. Alaee, A. G. Lamprianidis, D. Beutel, R. W. Boyd, C. Rockstuhl, *Adv. Opt. Mater.* **2022**, *10*, 10.
[34] D. Beutel, I. Fernandez-Corbaton, C. Rockstuhl, *Comput. Phys. Commun.* **2024**, *297*, 109076.
[35] B. Schaefer, E. Collett, R. Smyth, D. Barrett, B. Fraher, *Am. J. Phys.* **2007**, *75*, 163.
[36] E. Noponen, J. Turunen, *J. Opt. Soc. Am. A* **1994**, *11*, 2494.
[37] *Electromagnetic Theory of Gratings*, Springer Berlin Heidelberg, Berlin Heidelberg **1980**.
[38] M. V. Gorkunov, A. A. Antonov, Y. S. Kivshar, *Phys. Rev. Lett.* **2020**, *125*, 093903.
[39] A. Overvig, N. Yu, A. Alú, *Phys. Rev. Lett.* **2021**, *126*, 073001.
[40] B. Semnani, J. Flannery, Z. Ding, R. A. Maruf, M. Bajcsy, in *Conference on Lasers and Electro-Optics*, CLEO_QELS. OSA, **2019**, FM1B.1.
[41] S. Wang, Z.-L. Deng, Y. Wang, Q. Zhou, X. Wang, Y. Cao, B.-O. Guan, S. Xiao, X. Li, *Light: Sci. Appl.* **2021**, *10*, 1.